NOTES AND CORRESPONDENCE

The Spindown of Bottom-Trapped Plumes

RICARDO P. MATANO

College of Oceanic and Atmospheric Sciences, Oregon State University, Corvallis, Oregon

ELBIO D. PALMA

Departamento de Fisica, Universidad Nacional del Sur, and Instituto Argentino de Oceanografía (CONICET), Bahia Blanca, Argentina

(Manuscript received 1 September 2009, in final form 14 January 2010)

ABSTRACT

This note considers the decay of a bottom-trapped freshwater plume after the causative freshwater inflow has ceased. It is shown that shortly after the low-density inflow stops, the barotropic pressure field that it created radiates away and the ocean circulation becomes controlled by baroclinic pressure gradients generated by the remnants of the inflow. This produces a reversal of the circulation in the region downstream of the inflow, after which the entire plume starts to move in the upstream direction. The decay of the plume is henceforth controlled by upstream oceanic flow and dilution through cross-isopycnal mixing.

1. Introduction

In an accompanying article, we investigate the causes for the upstream spreading (i.e., in the direction opposite to that of the propagation of coastally trapped waves) of bottom-trapped plumes (Matano and Palma 2010; hereafter MP10). There, we argue that this phenomenon follows the geostrophic adjustment of the flow, which generates a baroclinic pressure field and geostrophically balanced upstream currents that advect the density anomalies in that direction. In this note, we further explore this theme by considering the spindown of a bottom-trapped plume; that is, the history of the plume after the freshwater inflow is terminated.

There are several studies on the decay and relaxation of buoyant plumes, but most of them have been focused on either surface-trapped plumes or in the region where the estuary containing the freshwater source connects to the open ocean. Chao (1988) studied the spindown of surface-trapped plumes produced within an estuary and concluded that there was ''no significant visual difference [with the forced case] over the shelf.'' The most significant changes occurred within the estuary. Valle-Levinson et al. (1996) investigated the effects of modifying the seaward discharge within a wide estuary and concluded that, when the pulse of buoyant water stops, the volume exchange with the shelf reverts from outflow dominated to a balance between inflow and outflow in the downstream region. Yankovsky et al. (2001) investigated the impact of inflow fluctuations and concluded that, although high-frequency oscillations have little effect on the plume dynamics, subinertial oscillations substantially modify the anticyclonic bulge that forms at the river mouth.

To the best of our understanding, no study has addressed the processes controlling the decay of bottom-trapped plumes, particularly in the far field and for relatively long time scales ($T > 10$ days). Bottom-trapped plumes are distinguished by the fact that their characteristics (spreading rate, width, etc.) are highly influenced by the slope of the bottom topography (e.g., Whitehead and Chapman 1986; Chapman and Lentz 1994; Kourafalou et al. 1996; Yankovsky and Chapman 1997; Avicola and Huq 2002; Lentz and Helfrich 2002). Our goal here is to determine the dynamical mechanisms controlling the temporal evolution of a bottom-trapped plume after the causative freshwater source is removed. Is the spindown

Corresponding author address: Ricardo P. Matano, College of Oceanic and Atmospheric Sciences, Oregon State University, 104 COAS Administration Building, Corvallis, OR 97331-5503.
E-mail: rmatano@coas.oregonstate.edu

DOI: 10.1175/2010JPO4352.1

of the plume controlled by the same circulation patterns developed during its growth? For example, do the remnants of the inflow continue dispersing in the downstream and upstream directions or does a new circulation pattern emerge? We address these questions by extending MP10's benchmark experiment with the buoyancy source turned off. As we shall show, the processes controlling the spindown of this type of plume is relevant not only to our understanding of the plume's response to time varying forcing but also to the generation of upstream flows. In the next section, we describe the model configuration used in this study.

2. Model description

The numerical model used in this study is the Princeton Ocean Model (Blumberg and Mellor 1987). The model domain, which is set in the Southern Hemisphere, consists of a rectangular basin 400 km long (y direction) and 80 km wide (x direction). The model has a horizontal resolution of 2.5 km in the alongshore direction, 1.25 km in the cross-shore direction, and 25 sigma levels in the vertical with enhanced resolution near the surface and the bottom. The bottom topography consists of a shelf with constant slope and no meridional variations. Bottom friction is parameterized with a quadratic friction law with variable drag coefficient. There are three open boundaries on the southern, northern, and eastern sides of the domain, where we impose the conditions recommended by Palma and Matano (1998, 2000). The western boundary is closed, except for the locus of freshwater inflow, where we impose a freshwater source in the continuity equation following the scheme of Kourafalou et al. (1996). At the inlet, there is a source of low-density fluid with a density anomaly of -1.0 kg m^{-3} and a fixed discharge rate of $Q =$ 24 000 m^3 s^{-1}. The upstream edge of the inlet is located at $y = 195$ km, and its width is $L = 17.5$ km.

In the first experiment to be described (EXP1 in MP10), the ocean is initially quiescent and of constant reference density ρ_o; the Coriolis parameter is set at $f = -10^{-4}$ s^{-1}; the coefficients of vertical eddy viscosity K_M and diffusivity K_H are computed using the Mellor–Yamada 2.5 turbulent closure scheme (Mellor and Yamada 1982). This experiment does not include bottom friction. The depth of the basin is 15 m at the coast and increases linearly cross-shore with bottom slope $\alpha = 2 \times 10^{-3}$. The buoyant discharge is held constant through the first 30 days of numerical integration, after which it is shut off and the model is let to freely evolve for an additional 60 days.

3. Results

Although this article is mainly concerned with the spindown period, for the purposes of completeness we also include a brief description of the spinup. A detailed discussion can be found in MP10.

a. The spinup

Initially, the freshwater spreads isotropically around the inlet until the scale of the perturbation grows sufficiently for rotation effects to become important; hence, the dynamical adjustment of the downstream and upstream portions of the shelf follow different paths. The adjustment in the downstream region starts with the generation and propagation of coastally trapped waves, traveling with the coast to their left and leaving in their wake a geostrophically adjusted alongshelf current that advects the density anomaly away from its source. The adjustment in the upstream region starts near the inlet where the discharge generates a positive baroclinic pressure gradient and, through geostrophic equilibrium, an upstream flow that advects less dense fluid in a self-sustaining motion. The freshwater discharge generates upstream flows at both sides of the inlet; in the downstream region, this upstream flow manifests as a deep countercurrent (MP10). The rate of downstream spreading is faster than that of upstream spreading, but the latter is a persistent phenomenon that diverts approximately half of the freshwater discharge onto the shelf (MP10).

b. The spindown

To illustrate the differences between the spinup and spindown periods, we constructed a Hovmöller diagram of the minimum surface density anomaly at each cross-shelf section (Fig. 1). The spinup period (days 1–30) is characterized by downstream and upstream spreading of the discharge (MP10). The spindown period (days 30–90) is characterized by a rapid reversal of the downstream spreading trends, followed by an overall upstream displacement at both sides of the inlet. This reversal is marked by the change of slope of the isopycnals at day 30, after which the entire plume moves upstream. Thus, although during the growth phase there is downstream as well upstream propagation, during the spindown phase there are only upstream displacements. There are two clearly defined time scales in the Hovmöller diagram: a long time scale associated with the upstream displacement of the nose of the plume (line A of Fig. 1) and a short time scale associated with the upstream advection of the remains of the density anomaly (lines B and C of Fig. 1). The former is nearly uniform during the entire simulation period and is associated with the processes described in MP10. The latter changes visibly with time and is associated with advective processes generated by the baroclinic pressure gradient (MP10). The decrease of the upstream velocities during the spindown processes reflects the effects of mixing on the plume density structure.

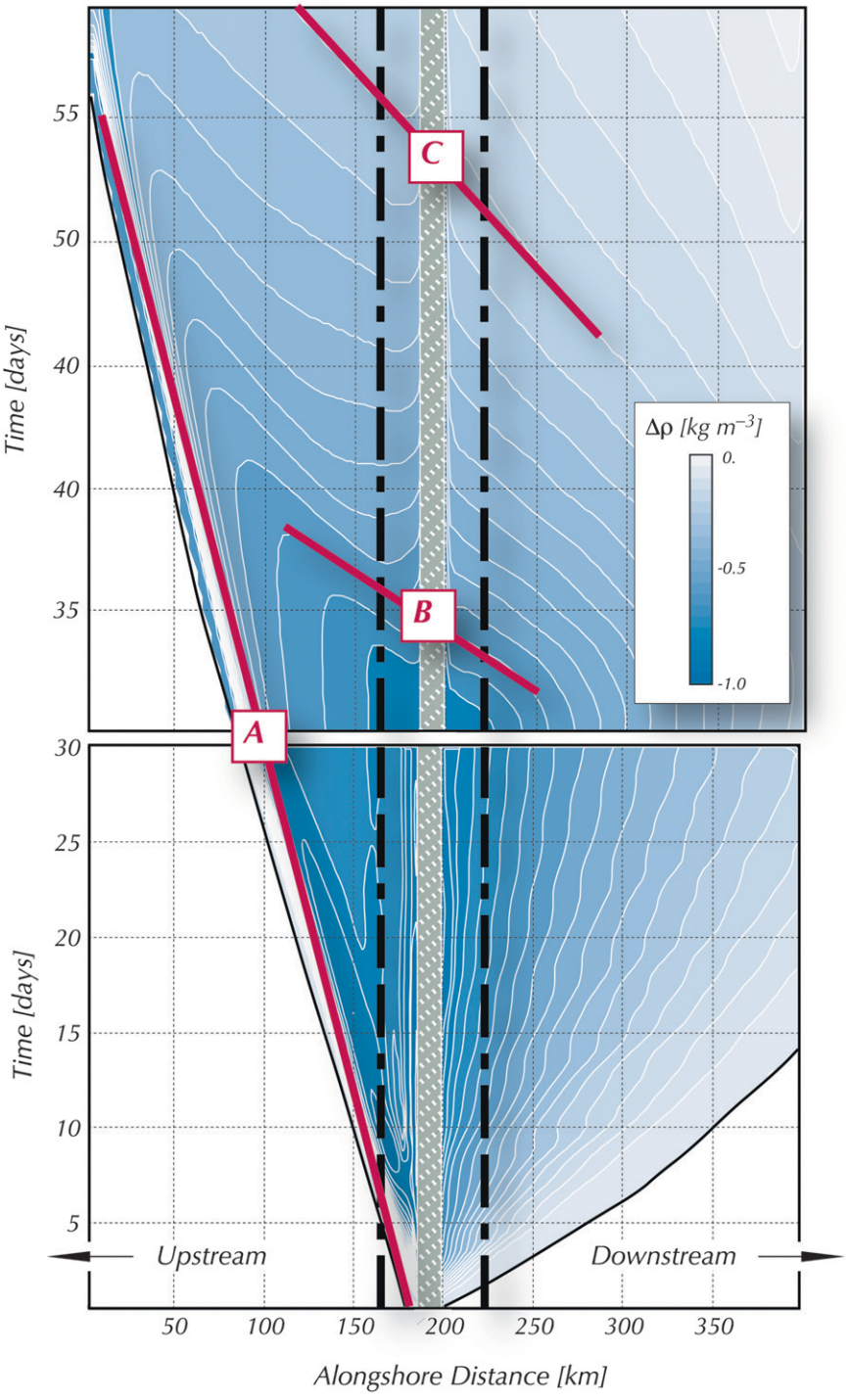

FIG. 1. Hovmöller diagram of the minimum surface density at each cross-shelf section. The crosshatch marks the location of the outflow discharge. The spinup encompasses days 1–30, and the spindown encompasses days 30–60. The slope of the red lines corresponds with the propagation speeds of (a) the upstream nose of the plume, (b) the interior fluid during the beginning of the spindown experiment, and (c) the interior fluid in the middle of the decay experiment.

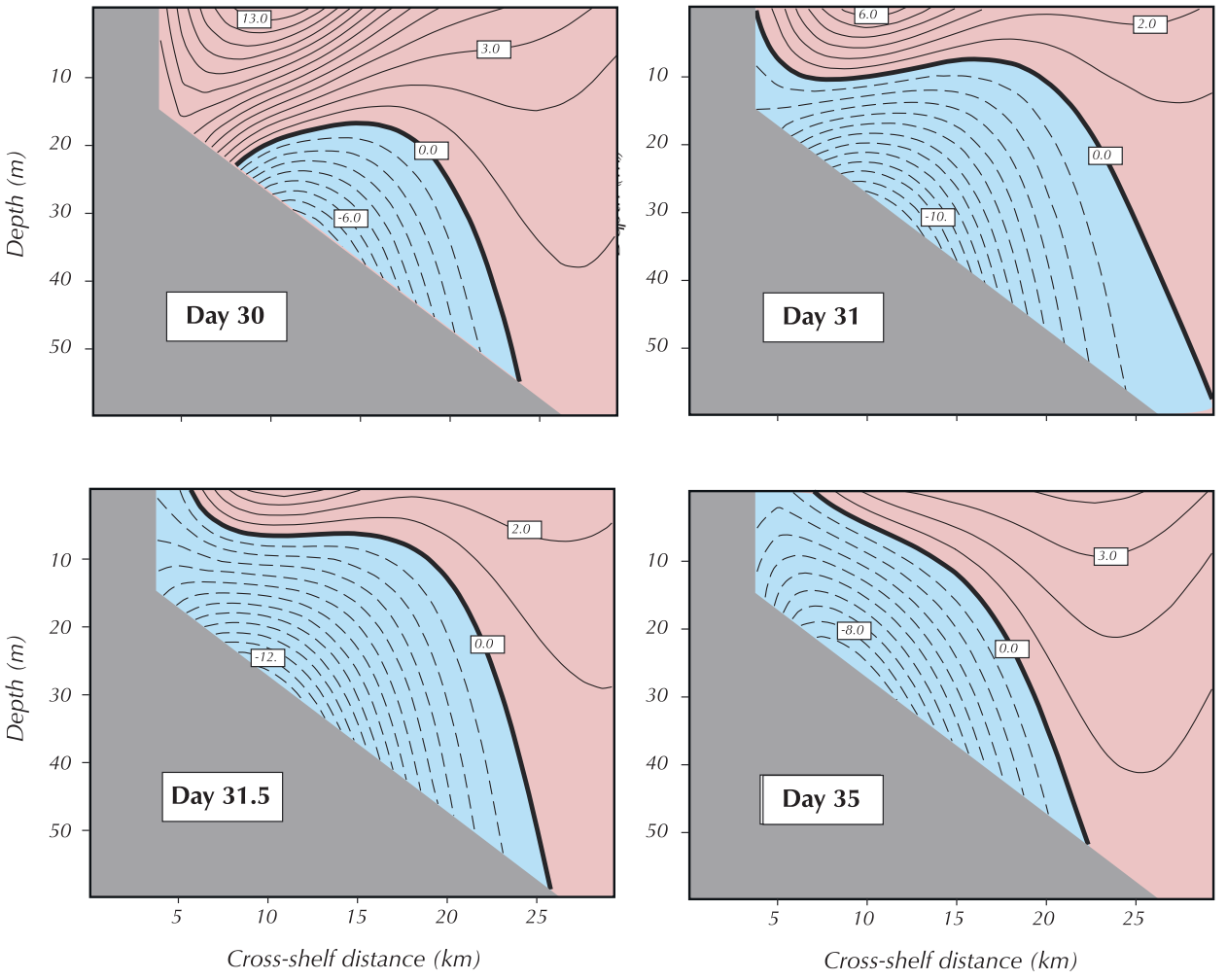

FIG. 2. Snapshots of the alongshelf velocity in the downstream cross section ($y = 225$ km) during the first five days of the spindown experiment. Units for velocity are cm s^{-1}. Positive values (red) correspond to velocities in the downstream direction.

Scale analysis suggests that the spindown of a buoyant plume has three well-defined time scales: a fast response that is associated with the downstream radiation of the barotropic pressure gradient setup by coastally trapped waves, an intermediate-time response that is associated with the upstream advection of the density anomalies, and a slow response that is associated with mixing processes. For the model configuration used in this study, the fast response could be estimated from the time it takes a coastally trapped wave to cross the domain. Using the values from our model (i.e., $f = 10^{-4}$ s^{-1}, $\alpha = 2 \times 10^{-3}$, $h = 20$ m, $L_x = 100$ km, and $L = 200$ km), the wave speed can be approximated as (e.g., Brink 1991)

$$C = \frac{f\dfrac{\alpha}{h}}{(2\pi/L_x)^2} \approx \frac{10^{-4}\dfrac{10^{-3}}{20}}{(2\pi/2 \times 10^5)^2} \approx 1.3\,\text{m s}^{-1} \Rightarrow T = \frac{L}{C} \approx 1 - 2\ \text{days}.$$

The intermediate response is the time required to move the density anomaly away from the domain. Assuming that the plume moves at approximately the speed of the fluid (a typical speed of 0.1 m s^{-1}; MP10), the advective time scale is

$$T \approx \frac{200\,000\,\text{m}}{0.1\,\text{m s}^{-1}} \approx 3\,\text{weeks}.$$

The slow response is determined by mixing processes. Assuming that vertical mixing controls the spindown of the density anomaly, then $T \approx h^2/K_\rho$, where h is a coastal depth ($h \sim 20$ m) and K_ρ is the vertical mixing coefficient. The magnitude of K_ρ is difficult to estimate, but values of 1×10^{-5} m^2 s$^{-1} < K_\rho < 1 \times 10^{-4}$ m^2 s^{-1} give a time scale of 1 month $< T <$ 1 yr. These rough estimates indicate that the advective and mixing time scales are close enough so that there should be a significant dilution of the plume as it is advected.

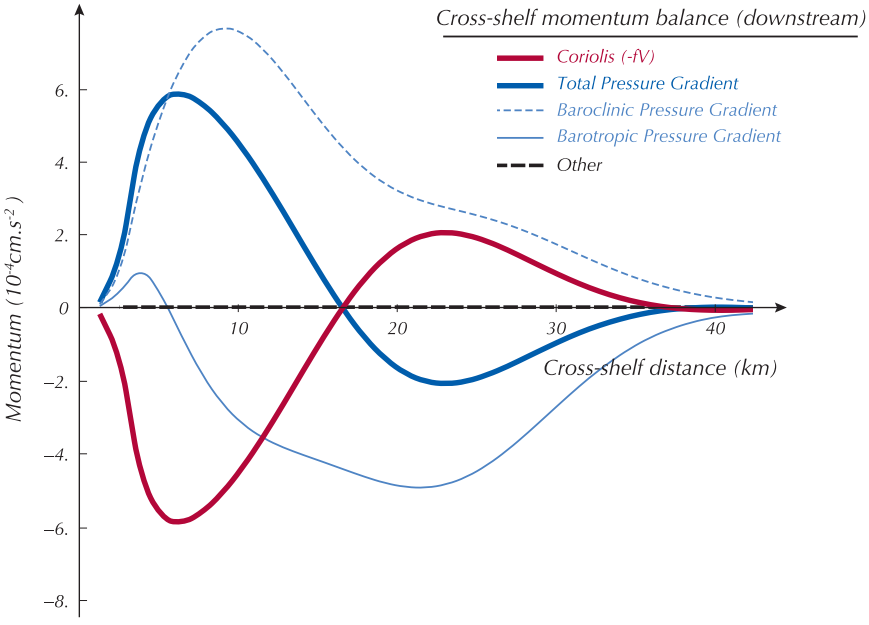

FIG. 3. Cross-shelf component of the vertically averaged momentum balance in the downstream cross section (y = 225 km) at day 35.

The previous analysis indicates that, although on long time scales (months), mixing should be ultimately responsible for the demise of the plume; on short time scales (hours to weeks) the plume's characteristics should be controlled by wave propagation and advection. These predictions are in good agreement with the results of our experiment, showing that the first phase of the spindown process is dominated by wave propagation and the subsequent phases are dominated by advection and mixing. Thus, after the inlet is closed, coastally trapped waves radiate away most of the energy of the barotropic pressure field, leaving in their wake a baroclinic pressure gradient that generates upstream currents at both sides of the inlet. Subsequently, all remnants of the plume are advected in the upstream direction until the signal leaves the domain (through the upstream boundary).

To characterize the different phases of the spindown, we will focus first on the fast response, which encompasses the first 36 h of the extended simulation. During this period, the radiation of coastally trapped waves weakens the barotropic pressure gradient and the coastal dynamics become dominated by the baroclinic pressure gradient set by the cross-shelf density differences. These processes are most evident in the evolution of the inner-shelf velocities in the downstream region, which during the growth period are largely controlled by the barotropic pressure gradient (MP10). At day 30, the start of the spindown experiment, the vertical structure of the alongshelf velocity is similar to that depicted by Chapman and Lentz (1994) and consists of a downstream flow in the upper layers and a countercurrent deep below (Fig. 2). The downstream flow is generated by the barotropic pressure gradient associated with the cross-shelf sea surface height (SSH) gradient, while the deep undercurrent is generated by the baroclinic pressure gradient associated with the cross-shelf density gradient (e.g., Fig. 12 of MP10). After the freshwater influx is stopped, coastal waves drain the energy from the barotropic pressure field and the inner-shelf dynamics become dominated

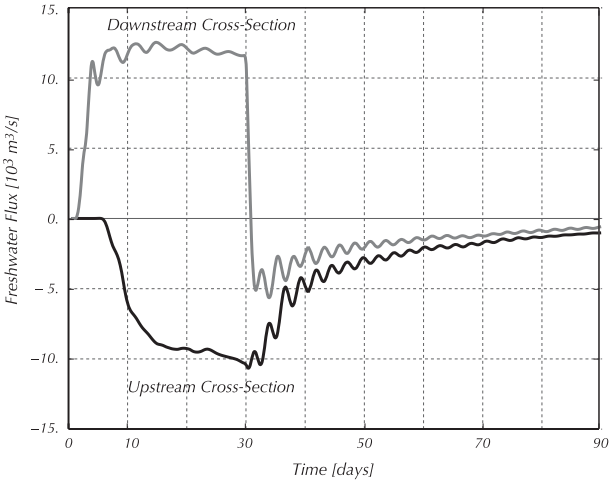

FIG. 4. Time series of the freshwater fluxes in the upstream and downstream cross sections. The location of the cross sections is marked by the dotted lines in Fig. 1. The definition of the freshwater fluxes can be found in MP10.

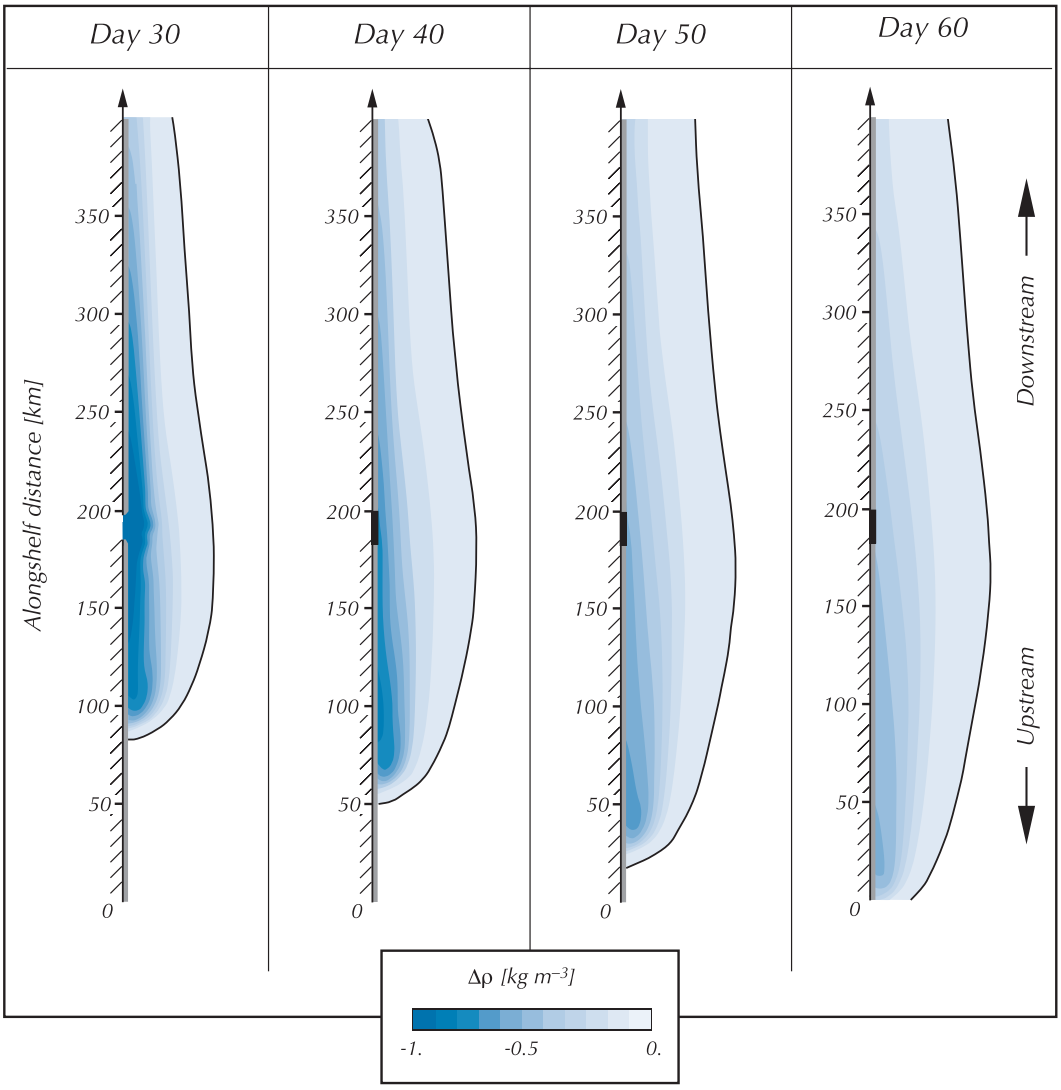

FIG. 5. Snapshots of the surface density anomalies (kg m^{-3}) during the first 30 days of the spindown experiment.

by the baroclinic pressure gradient. At day 31, for example, we observe a weakening of the downstream velocities and a strengthening of the upstream velocities (Fig. 2). A few hours later (day 31.5), the upper-layer velocities reverse direction in the region closest to the coast where all the flow is now directed in the upstream direction. In the following days, this tendency is accentuated and by day 35; for example, the downstream region has a velocity structure that is very similar to that observed in the upstream region (e.g., Fig. 7 in MP10). That is, there is a bottom intensified upstream flow in the inner shelf and a weak surface intensified return flow farther offshore. The decay of the barotropic pressure gradient and the dominance of the baroclinic pressure gradient on the alongshelf velocities are clearly evident in the cross-shelf momentum balance (Fig. 3). Note that not all the barotropic pressure gradient disappears, but only that portion close to the coast, which is set up by the coastally trapped waves. The changes of the upstream velocity field just described produce a reversal of the freshwater flux in the downstream region (Fig. 4). During the spinup (days 1–30), the total freshwater input is approximately equipartitioned between the upstream and downstream regions (MP10). However, soon after the inlet is closed, the net freshwater flux in the downstream region is directed upstream.

The evolution of the plume after the inlet is closed is illustrated with snapshots of the sea surface density anomaly (Fig. 5). After the reversal of the alongshelf velocities in the downstream region, the entire plume

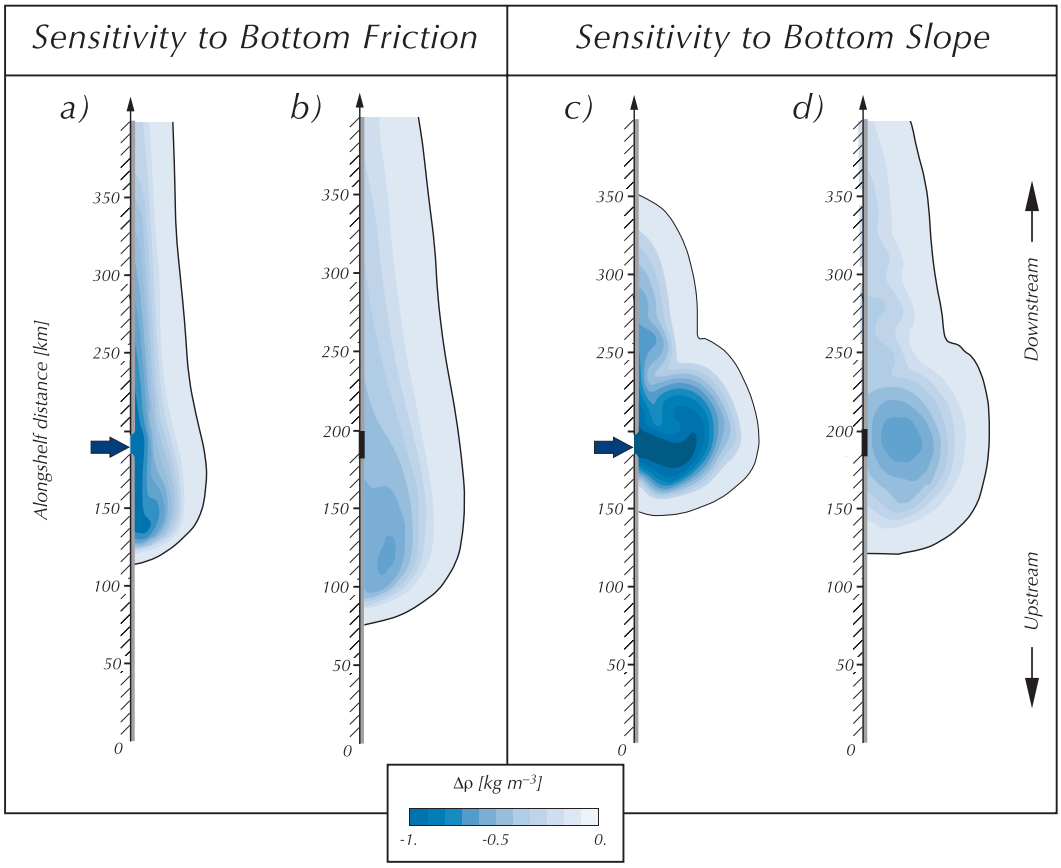

FIG. 6. Snapshots of the surface density anomalies (kg m^{-3}) in the sensitivity experiments: (a) day 30 (end of the spinup) of the experiment using bottom friction; (b) day 60 (spindown) of the experiment using bottom friction; (c) day 30 (end of the spinup) of the experiment using a flat-bottom basin; (d) day 60 (spindown) of the experiment using a flat-bottom basin.

starts to move in the upstream direction. By day 40, for example, the minimum density anomaly has been displaced upstream of the inlet; by day 50, it is located at the forefront of the plume. As the plume advances, it gets noticeably diluted. The dilution is faster than that predicted from our simple scaling arguments because of the contribution of advective effects. The density structure at any single point is largely determined by a balance between alongshelf advection, which imports low-density waters, and offshore advection, which exports low-density waters. As the alongshelf density gradient starts to decrease because the freshwater source has been shut off, the offshore export weakens the cross-shelf density gradient, broadening and diluting the density anomaly. These effects are clearly manifested in the snapshots of days 50 and 60, which show a cross-shelf broadening of the isopycnals. As the plume gets diluted, it moves at a slower speed, and this effect can be clearly appreciated in the change of slope of the isopycnals in the Hovmöller diagrams of surface densities (lines B and C of Fig. 1). By day 90 (the end of our simulation), most of the density anomaly has already left the domain.

In MP10 we show that, although upstream spreading is a relatively robust process, the magnitude of the spreading is sensitive to the development of a bottom boundary layer. Thus, experiments including bottom friction develop slower upstream intrusions. To characterize the effects of bottom friction during the spindown period, we repeated the previous experiment using the bottom friction described in MP10. The results show upstream intrusions that move more slowly and are wider but are not otherwise qualitatively different from the previous case (Figs. 6a,b). The widening of the plume in the upstream region follows the development of a bottom boundary layer that strengthens the cross-shelf circulation patterns. Thus, in this experiment there is a stronger offshore advection of low-density waters in the upper layers and stronger onshore advection of high-density waters in the bottom layers (e.g., MP10). The only experiments where upstream spreading did not occur

were those conducted in a flat-bottomed basin (Figs. 6c,d). In these cases, most of the discharge is funneled to a radially spreading bulge (Fig. 6c), which diffuses away during the spindown period (Fig. 6d).

4. Conclusions

The spindown of a buoyant plume clearly demonstrates the importance of the baroclinic pressure gradient in the generation of upstream intrusions. Buoyant anomalies generate a pressure force that pushes the fluid in the upstream direction when the density of the discharge is smaller than the density of the environment (MP10). The barotropic pressure field set up by the coastally trapped waves drives the downstream displacements that occur even if the discharge has no density anomaly (e.g., Yankovsky 2000; MP10). The upstream effects generated by this type of inflow are evident in the spindown experiment just described. Shortly after the inflow ceases, the barotropic pressure field created by the discharge radiates away and the circulation becomes controlled by the baroclinic pressure gradients generated by the remnants of the low-density inflow. This produces a reversal of the alongshelf currents in the downstream region, after which the entire plume starts to move in the upstream direction. The decay of the plume henceforth is controlled by outflow through the upstream boundary and dilution through cross-isopycnal mixing.

Acknowledgments. This article greatly benefited from the insightful comments and suggestions of Dr. A. Yankovsky and an anonymous reviewer. R. P. Matano acknowledges the financial support of the National Science Foundation through Grants OCE-0726994 and OCE-0928348 and of NASA through Grant NNX08AR40G. E. D. Palma acknowledges the financial support from CONICET (PIP09-112-200801), Agencia Nacional de Promoción Científica y Tecnológica (PICT08-1874), Universidad Nacional del Sur (24F044), and the Inter-American Institute for Global Change Research, supported by the U.S. National Science Foundation Grant GEO-045325.

REFERENCES

Avicola, G., and P. Huq, 2002: Scaling analysis for the interaction between a buoyant coastal current and the continental shelf: Experiments and observations. *J. Phys. Oceanogr.,* **32,** 3233–3248.

Blumberg, A. F., and G. L. Mellor, 1987: A description of a three-dimensional coastal ocean circulation model. *Three-Dimensional Coastal Ocean Models,* N. Heaps, Ed., Coastal Estuarine Science Series, Vol. 4, Amer. Geophys. Union, 1–16.

Brink, K. H., 1991: Coastal-trapped waves and wind-driven currents over the continental shelf. *Annu. Rev. Fluid Mech.,* **23,** 389–412.

Chao, S.-Y., 1988: River-forced estuarine plumes. *J. Phys. Oceanogr.,* **18,** 72–88.

Chapman, D. C., and S. J. Lentz, 1994: Trapping of coastal density front by the bottom. *J. Phys. Oceanogr.,* **24,** 1464–1479.

Kourafalou, V. H., L.-Y. Oey, J. D. Wang, and T. N. Lee, 1996: The fate of river discharge on the continental shelf 1. Modeling the river plume and inner shelf coastal current. *J. Geophys. Res.,* **101,** 3415–3434.

Lentz, S. J., and K. R. Helfrich, 2002: Buoyant gravity currents along a sloping bottom in a rotating fluid. *J. Fluid Mech.,* **464,** 251–278.

Matano, R. P., and E. D. Palma, 2010: The upstream spreading of bottom-trapped plumes. *J. Phys. Oceanogr.,* **40,** 1631–1650.

Mellor, G. L., and T. Yamada, 1982: Development of a turbulent closure model for geophysical fluid problems. *Rev. Geophys. Space Phys.,* **20,** 851–868.

Palma, E. D., and R. P. Matano, 1998: On the implementation of open boundary conditions for a general circulation model: The barotropic mode. *J. Geophys. Res.,* **103,** 1319–1341.

——, and ——, 2000: On the implementation of open boundary conditions for a general circulation model: The three-dimensional case. *J. Geophys. Res.,* **105** (C4), 8605–8627.

Valle-Levinson, A., J. M. Klinck, and G. H. Wheless, 1996: Inflows/outflows at the transition between a coastal plain estuary and the coastal ocean. *Cont. Shelf Res.,* **16,** 1819–1847.

Whitehead, J. A., and D. C. Chapman, 1986: Laboratory observations of a gravity current on a sloping bottom: The generation of shelf waves. *J. Fluid Mech.,* **123,** 237–266.

Yankovsky, A. E., 2000: The cyclonic turning and propagation of buoyant coastal discharge along the shelf. *J. Mar. Res.,* **58,** 585–607.

——, and D. C. Chapman, 1997: A simple theory for the fate of buoyant coastal discharges. *J. Phys. Oceanogr.,* **27,** 1386–1401.

——, B. M. Hickey, and A. K. Münchow, 2001: Impact of variable inflow on the dynamics of a coastal buoyant plume. *J. Geophys. Res.,* **106** (C9), 19 809–19 824.